Aqueous Organic Pollutants

Subjects: Engineering, Mechanical

Contributor: Maria Jose Martin De Vidales

Advanced oxidation processes (AOPs) are regarded as effective techniques for organic contaminants removal from water and wastewater.

Keywords: graphitic carbon nitride ; AOPs

1. Introduction

In recent years, environmental pollution, especially water pollution, is increasingly becoming a major concern worldwide. Many organic pollutions, such as pharmaceuticals and personal care products (PPCPs), pesticides, and organic dyes are toxic and refractory [1][2][3][4]. Various techniques have been developed to eliminate aqueous organic pollutants (e.g., extraction, adsorption, biological treatment, and advanced oxidation processes) [5][6][7][8][9]. Advanced oxidation processes (AOPs) are regarded as effective techniques for organic contaminants removal from water and wastewater [10][11][12][13][14].

The AOPs utilize highly reactive species (mainly hydroxyl radical, •OH) to oxide the organic pollutants into less toxic or no-toxic products such as CO_2 and H_2O [15][16]. According to supplied energies and reactive species, AOPs can be categorized as photocatalysis, electrocatalysis, sonolysis, ozonation, Fenton/Fenton-like reactions, and sulfate radical-based AOPs (SR-AOPs), among others [17][18]. In recent decades, numerous studies have been conducted to develop novel AOPs. Emerging energy sources (e.g., ionizing radiation with electron beams and γ-radiolysis, pulsed plasma, etc.) were applied, and different reactive species (such as periodate or ferrate reagent) were introduced [19][20][21][22]. Considering the merits of different AOPs, combinations of various processes are more common approaches to enhance degradation efficiency [21]. Although some AOPs (e.g., UV/H_2O_2, UV/peroxymonosulfate (PMS)) work properly without catalysts, employing catalysts can significantly reduce energy and reagent (source of reactive species) consumption [23]. Therefore, designing an effective and stable catalyst is a crucial strategy for the development of AOPs.

Graphic carbon nitride (g-C_3N_4), known as a metal-free polymer semiconductor, has attracted increasing attention due to its unique electronic band structure, anti-photocorrosion, excellent physicochemical stability, and easy availability [24][25]. The bandgap of g-C_3N_4 is about 2.7 eV, which enables it to absorb all viewing range of solar irradiation. The valance band (VB) and conduction band (CB) mainly encompass nitrogen and carbon p_z orbitals while VB top and CB bottom are located at about +1.4 and −1.3 eV, respectively [26][27][28]. The study of g-C_3N_4 can be traced back to 1834, when Berzelius first synthesized a polymeric derivative of g-C_3N_4, and Liebig named it melon [29]. In 2006, Goettmann and his co-workers investigated Friedel–Crafts reactions that can be catalyzed by g-C_3N_4, which is its first application in the catalytic field [30]. In 2009, g-C_3N_4 was demonstrated as a good metal-free photocatalyst for water splitting by Wang et al. [26]. Up to now, g-C_3N_4 has been in-depth studied and extensively applied in photocatalysis. The g-C_3N_4 preparation relies on (solvo)thermal polymerization of nitrogen-rich precursors such as melamine, dicyandiamide, and urea [31]. In addition, hard/soft temple-assisted methods and sol-gel methods are frequently used to modify the synthesis approaches. The reaction parameters such as precursors and temperature could significantly affect the physicochemical property, including specific surface area, bandgap, etc. [32]. However, the pure g-C_3N_4 encounters several drawbacks, including tiny surface area, inefficient use of visible light, low electric conductivity, and fast recombination of photo-induced carriers, which are not beneficial to its catalytic activity [33][34]. To address these issues, a lot of efforts such as (1) engineering the nanostructure of g-C_3N_4 [27][35][36][37], (2) introducing heteroatoms (metals [38][39][40][41][42][43][44] or non-metals [45][46][47][48][49][50]), (3) coupling with other semiconductors [51][52][53][54][55][56][57] and (4) co-polymerization [58][59][60][61] were made. g-C_3N_4 based composites hold unique advantages for organic pollutants removal from groundwater and wastewater due to the good adsorption capacity of g-C_3N_4 for organic molecules, which could be attributed to strong intermolecular forces like hydrogen bonding, π-π interactions between pollutant molecules and residual amino groups in the g-C_3N_4 fragment [62][63]. On the other hand, introducing extra sources of reactive species such as H_2O_2 or PMS in photocatalysis can significantly increase degradation efficiency [64][65]. Furthermore, some studies have explored g-C_3N_4 based composites for organic pollutants removal without light irradiation in the presence of PMS or H_2O_2 [66][67][68][69].

Some excellent reviews on g-C_3N_4 based composites involving pollution remediation have been published [25][31][70][71]. g-C_3N_4 based composites as photocatalysts for water purification have been summarized in these reviews, while no reviews involve other AOPs such as chemical AOPs and electrochemical AOPs. The dramatically increasing amounts of g-C_3N_4 based composites in the range of AOPs fields requires a broader, thorough, and up-date assessment.

2. Chemical AOPs

The chemical AOPs started as early as the application of the Fenton reaction to water treatment, in which •OH can be generated from the catalytic decomposition of H_2O_2 by Fe^{2+} for the destruction of various organic pollutants (Equation (1)) [10].

$$Fe^{2+} + H_2O_2 + H^+ \rightarrow Fe^{3+} + \bullet OH + H_2O \quad (1)$$

With the increasing demand for water treatment, various oxidants such as O_3, PMS, peroxydisulfate (PDS) were applied in chemical AOPs. The PMS and PDS could be heterogeneous activated, and reactive species such as $\bullet SO_4^-$ are subsequently generated to degrade organic pollutants [72][73][74]. Table 1 summarizes the part of a representative study using g-C_3N_4 based composites as a catalyst in chemical AOPs.

Table 1. Graphic carbon nitride (g-C_3N_4) based composites for chemical advanced oxidation processes (AOPs).

Catalyst	Target Contaminants	Oxidant	Reaction Conditions	Performance	Ref.
Cu(II)/$CuAlO_2$/g-C_3N_4	Bisphenol A (BPA)	H_2O_2	BPA, 25 mg/L; catalyst, 1 g/L; H_2O_2, 10 mM; T, 35 °C; pH, 7	95.5% in 120 min	[75]
Cu/Al_2O_3/g-C_3N_4	Rhodamine B (RhB)	H_2O_2	RhB, 20 mg/L; catalyst, 1 g/L; H_2O_2, 10 mM; T, 25 °C; pH, 4.9	96.4% in 100 min	[76]
Iron oxide/g-C_3N_4	Ciprofloxacin	H_2O_2	ciprofloxacin, 20 mg/L; catalyst, 1 g/L; H_2O_2, 5.6 mM; pH, 3	100% in 60 min	[68]
g-C_3N_4/carbon nanotubes/Fe(II)	Methylene blue	H_2O_2	Methylene Blue, 90 mg/L; catalyst, 0.5 g/L; H_2O_2, 1 mM; T, 25 °C; pH, 4.9	66.8% in 1 h	[69]
Fe_3O_4@C/g-C_3N_4	Acid orange 7 (AO 7)	PMS	AO 7, 20 mg/L; catalyst, 0.6 g/L; PMS, 0.1 g/L; T, 25 °C; pH, 4	97% in 20 min	[77]
$CoFeO_2$/g-C_3N_4	Levofloxacin	PMS	levofloxacin, 10 mg/L; catalyst, 0.15 g/L; PMS, 0.5 mM; T, Room temperature; pH, 3	100% in 60 min	[78]
Co-doped g-C_3N_4	4-chlorophenol	PMS	4-chlorophenol, 50 mg/L; catalyst, 1 g/L; PMS, 2.5 mM	100% in 30 min	[79]
Mn-doped g-C_3N_4	Acetaminophen	PMS	acetaminophen, 20 mg/L; catalyst, 0.05 g/L; PMS, 0.8 g/L; pH, 6.5	100% in 15 min	[80]
Cu^+-g-C_3N_4	Rhodamine B	H_2O_2	Rhodamine B, 50 mg/L; catalyst, 0. 8 g/L; H_2O_2, 40 mM; pH, neutral	99.2% in 1 h	[81]
Pd/g-C_3N_4	BPA	PMS	BPA, 20 mg/L; catalyst, 0.1 g/L; PMS, 1 mM; T, 25 °C; pH, 9	91% in 60 min	[82]
FeO_y/S-g-C_3N_4	Sulfamethoxazole	PMS	sulfamethoxazole, 10 mg/L; catalyst, 0.5 g/L; PMS, 0.8 mM; T, 25 °C; pH, 3.54	100% in 60 min	[83]
Fe(III)-doped g-C_3N_4	AO 7	PMS	AO 7, 8.5 mg/L; catalyst, 0.1 g/L; PMS, 0.1 g/L; pH, 3–4	97% in 30 min	[84]
cryptomelane-type manganese oxide/g-C_3N_4	AO 7	PMS	AO 7, 0.13 mM; catalyst, 0.2 g/L; PMS, 0.65 mM; T, 8 °C; pH, 7.25	88% in 30 min	[85]
carbon and oxygen dual-doped g-C_3N_4	BPA	PMS	BPA, 0.1 mM; catalyst, 0.5 g/L; PMS, 5 mM; T, 30 °C; pH, 6.7	100% in 60 min	[86]
Active carbon/g-C_3N_4	AO 7	PMS	AO 7, 50 mg/L; catalyst, 0.2 g/L; PMS, 0.4 g/L; T, 27 °C; pH, 3.82	100% in 20 min	[87]
Fe-doped g-C_3N_4/graphite	4-chlorophenol	PMS	4-chlorophenol, 0.1 mM; catalyst, 0.1 g/L; PMS, 0.1 mM; pH, 3	100% in 10 min	[88]

Catalyst	Target Contaminants	Oxidant	Reaction Conditions	Performance	Ref.
Oxygen-doped g-C_3N_4	BPA	PMS	BPA, 0.05 mM; catalyst, 1 g/L; PMS, 10 mM; T, 30 °C; pH, 3–9	100% in 60 min	[66]
Fe(II)-doped g-C_3N_4	Phenol	PMS	phenol, 0.1 mM; catalyst, 1 g/L; PMS, 5 mM; T, 23 °C; pH, 2.6	100% in 20 min	[89]
Mn_3O_4/g-C_3N_4	4-chlorophenol	PMS	4-chlorophenol, 50 mg/L; catalyst, 0.3 g/L; PMS, 1 mM; T, 25 °C; pH, 4	100% in 40 min	[90]

Pure g-C_3N_4 holds inert activation performance of oxidants such as H_2O_2 and PMS. Considering that g-C3N4 has excellent affinity to entrap transition metal ions, metal doping is the main strategy for improving the catalytic activity. Oh et al. investigated the catalytic activities of Me-doped g-C_3N_4 (Me = Cu, Co, and Fe) as PMS activator for sulfathiazole degradation. Among the prepared catalyst, Co-doped g-C_3N_4 (0.59 wt% Co) exhibited the highest degradation efficiency for sulfathiazole, while excessive metal doping and surface defects (-C≡N) had a scavenging effect for $\bullet SO_4^-$ [91]. The authors further studied Fe-doped g-C_3N_4 for acid orange 7 degradation, and the non-radical pathway was proposed [84]. Li et al. prepared Fe doped g-C_3N_4 as PMS activator for phenolic compounds degradation. (Fe (V) = O) generated from the oxidation of Fe(III)-N was proposed as dominant reactive species [67]. In another work, Fe doped g-C_3N_4 was also employed in PMS activation for phenol degradation. Authors investigated the ratio of 46% and 54% of Fe (III) and Fe (II) via Mössbauer spectra, while the XPS survey spectra suggested the primary Fe on the surface of the catalyst was in the 3+ state. It was proposed that the Fe (II) complex heterolyzed at the O-O bond of activated PMS to form Fe (IV) = O, which was the primary active species [89]. In PMS/Mn-doped g-C_3N_4 system, superoxide radical was firstly generated due to the PMS bounding to the Mn-N site, and singlet oxygen produced by superoxide radical was proposed as the responsible reactive species for acetaminophen degradation [80]. Ma et al. synthesized Cu (I)-doped g-C_3N_4 for the removal of rhodamine B in a Fenton-like reaction. Cu (I) could be firmly embedded in g-C_3N_4 and reactive species produced by the interaction of H_2O_2 and Cu (I) [81]. The unique adsorption capacity of g-C_3N_4 for some organic pollutants also leads to superior degradation performance. Xie et al. investigated that different monochlorophenols isomers (2-chlorophenol, 3-chlorophenol, and 4-chlorophenol) could be degraded efficiently using Co-doped g-C_3N_4 as a catalyst in the presence of PMS. It was confirmed that the degradation rate was in the same order as the adsorption quantity [79]. This was attributed to the strong intermolecular forces between pollutant molecules and residual amino groups in the g-C_3N_4 fragment [92]. Pd-doped g-C_3N_4 was successfully synthesized by anchoring Pd nanoparticles on g-C_3N_4 using KBH_4 reduction method, which was regularly active for PMS activation toward bisphenol A removal [82]. Metal oxide such as manganese oxide [85][90] and iron oxide [68] decorated on g-C_3N_4 are also employed for organic pollutions degradation via activating H_2O_2 or PMS (Figure 1). Lyu et al. prepared Cu (II)/$CuAlO_2$/g-C_3N_4 composite as a Fenton-like catalyst. The Cu and C were investigated as dual reaction centers, and C-O-Cu acts as bridges to accelerating electrons transfer [75]. Nonmetal doping is also considered to be an efficient approach to improve electron transfer capability. Electronic structure modulation was achieved in oxygen-doped g-C_3N_4 for PMS activation, which was fabricated using urea and oxalic acid dihydrate [66]. The authors further investigated carbon and oxygen doped g-C_3N_4 exhibited better PMS activity due to its dual active sites-electron-poor C atoms and electron-rich O atoms [86]. Co-doping of iron and sulfur was found to be an approach to charge distribution and density of g-C_3N_4 for PMS activation [83]. To improve its chemical activity and electron transportation ability, Coupling nanocarbon materials g-C_3N_4 was developed to realize efficient PMS or H_2O_2 activation [87]. Moreover, combining nanocarbon materials and metal doping was frequently fabricated with g-C_3N_4 to exploit both materials' synergistic effect [69][77][88].

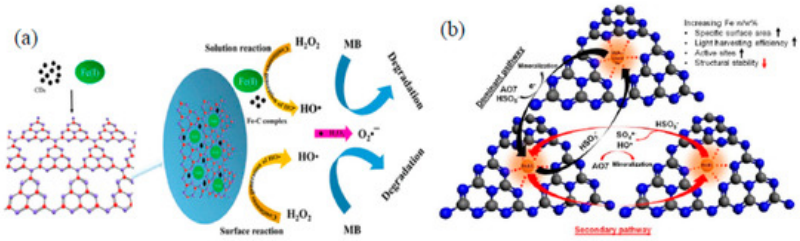

Figure 1. (**a**) Schematic illustration of the catalytic mechanism of g-C_3N_4/CDs/Fe(II) in the presence of H_2O_2, reprinted with permission from [68]. Copyright 2019 American Chemical Society. (**b**) Proposed mechanism of PMS activation by gCN-Fe_3 for AO7 removal, reprinted with permission from [83]. Copyright 2018 Elsevier.

3. Photochemical AOPs

Light irradiation is the most widely used method of applying additional energy to assist reactive species generating, which presents the advantages of simple, clean, relatively inexpensive, and efficient. TiO_2 and ZnO were firstly used as photocatalysts for catalytic oxidation of organic contaminants. In this case, photocatalysis induces the formation of h^+, $•O_2^-$ and •OH, which act as principle reactive species for pollutants degradation. Consequently, visible light irradiations have been coupled with powerful oxidants such as H_2O_2 and PMS, including catalysis with a modified photocatalyst, resulting in various AOPs. In this section, the applications of these different AOPs as photocatalysis, Photo-Fenton (like) reactions, and photo-assisted sulfate radical based AOPs are summarized. Some representative applications of g-C_3N_4 based composites as a catalyst in photochemical AOPs are shown in Table 2.

Table 2. g-C_3N_4 based composites for photochemical AOPs.

Catalyst	Target Contaminants	Light Source	Reaction Conditions	Performance	Ref.
$NiCo_2O_4$/g-C_3N_4	Carbamazepine	500 W Xenon lamp, Visible light	carbamazepine, 10 mg/L; catalyst, 0.5 g/L; PMS, 1 mM;	100% in 10 min	[93]
TiO_2/g-C_3N_4	Acetaminophen	300 W Xenon lamp, Visible light	acetaminophen, 5 mg/L; catalyst, 0.5 g/L; PS, 2 mM; pH, 7	100% in 30 min	[94]
Fe doped g-C_3N_4/graphene	Trimethoprim	350 W Xenon lamp, Visible light	Trimethoprim, 0.02 mM; catalyst, 0.5 g/L; PMS, 0.2 mM; pH, 6	100% in 120 min	[95]
MoS_2/A g/g-C_3N_4	Tetracycline	300 W Xenon lamp, Visible light	tetracycline, 20 mg/L; catalyst, 0.2 g/L; PMS, 0.1 mM; T, 20 °C; pH, 5.5	98.9% in 50 min	[96]
activated carbon/g-C_3N_4	Atrazine	300 W Xenon lamp, Visible light	atrazine, 5 mg/L; catalyst, 1 g/L; PMS, 5 mM; T, 25 °C; pH, 5.56	97.5% in 120 min	[97]
Cobalt-doped g-C_3N_4	Rhodamine B	500 W halogen tungsten lamp, Visible light	rhodamine B, 10 mg/L; catalyst, 0.4 g/L; PMS, 0.12 mM; T, 25 °C; pH, 4.68	100% in 25 min	[98]
Sulfur-doped/g-C_3N_4	Bisphenol A	150 W Visible light lamp	Bisphenol A, 50 mg/L; catalyst, 0.3 g/L; PMS, 0.3 g/L; T, 20 °C; pH, 5	85% in 120 min	[99]
g-C_3N_4-imidazole-based ligand-$FePcCl_{16}$	Carbamazepine	Xenon lamp, Visible light	carbamazepine, 25μM; catalyst, 0.1 g/L; PMS, 0.3 mM; pH, 7	95% in 25 min	[100]
Cu-modified alkalinized g-C_3N_4	Rhodamine B	halogen tungsten lamp, Visible light	rhodamine B, 10 mg/L; catalyst, 0.4 g/L; H_2O_2, 9.8 mM; pH, 4.6	95% in 10 min	[101]

3.1. Photocatalysis

As one typical technique of AOPs, photocatalytic degradation held the advantages of non-toxic, convenient operation, and high efficiency. With the irradiation of UV or visible light with energy larger than the semiconductor's energy gap, the electron-donating and electron-accepting sites are formed in the surface of the semiconducting catalyst. The photogenerated electrons migrate from the valence band (VB) to the corresponding conduction band (CB), leaving holes in the VB, resulting in the electrons and holes occupying the CB and VB, respectively. Holes can directly oxidize pollutants or react with H_2O/OH^- to produce hydroxyl radicals ($E^{\theta}_{(•OH/H2O)}$ = 2.8 eV/NHE). Whereas the electrons capture dissolved oxygen (O_2) to yield superoxide radical ($E^{\theta}_{(O2/•O2-)}$ = −0.3 eV/NHE). The resulting $•O_2^-$ are subsequently protonated to produce the •OH. Finally, those generated radicals take part in the oxidation of pollutants. In the early seventies, Fujishima and Honda showed the possibility of using the photo-excited semiconductor titanium dioxide (TiO_2) to split water into hydrogen and oxygen in a photo-electrochemical solar cell [102]. This fundamental work led to developing a new AOP technology, based on semiconductor photocatalysis, for water purification.

g-C_3N_4 compounds have emerged as up-and-coming candidates to replace TiO_2, owing to its graphite-like structure and medium bandgap [103][104]. However, the photocatalytic activity of g-C_3N_4 is still limited by its low electric conductivity and fast recombination of photo-induced carriers [105]. In this regard, modulating the nanostructure of g-C_3N_4 towards enhancing light harvest efficiency and catalytic mass-transfer is highly desirable. Researchers have made great efforts to design g-C_3N_4 with various structures, including 3D porous/nanospheres structure, 2D nanosheet and nanorod, etc. [27][37][106]. Such structures such as 3D porous and 2D nanosheet could provide high surface area, exposing more active sites

for catalytic surface reactions. Furthermore, nanostructured g-C_3N_4 could significantly reduce photo-induced carriers' transfer distance, leading to a lower recombination possibility. Moreover, the light quantum efficiencies could be significantly improved by constructing 0D, 1D nanorod, and 2D architectures g-C_3N_4 [107][108].

The VB top of g-C_3N_4 locates at about 1.4 V, leading to a small thermo-dynamic force for organic pollutants oxidation. Moreover, the more positive potential of •OH/H_2O standard redox voltage results the hole cannot directly oxidize the H_2O to generate •OH ($E^{\theta}_{(\bullet OH/H2O)}$ = 2.8 eV/NHE). To overcome this shortcoming, several elements of doping have been conducted [44][48][50][108]. Generally, metal doping occurs by inserting into the framework. In contrast, non-metal doping occurs in C or N atoms of g-C_3N_4 replaced by a heteroatom, which could enhance photocatalytic activity via improve the transfer and separation rates of photogenerated carriers and modulate bandgap [41][47]. Constructing heterojunction is another approach to enhance photodegradation performance for g-C_3N_4 [109][110]. Generally, Z-schemed heterojunction could be a good option that possesses higher redox potentials in forming reactive radicals and directly hole oxidation ability [111][112].

3.2. Photo-Fenton Like Processes

The Photo-Fenton process, the combination of ultraviolet or visible light with the conventional Fenton process, can enhance catalysts' catalytic capacity and increase the degradation efficiency of organic pollutants and reduce iron sludge production [113]. The successive and competitive steps reaction mechanism for the photo-Fenton process are shown in Equations (2) and (3).

$$Fe^{2+} + H_2O_2 \rightarrow Fe^{3+} + \bullet OH + HO^- \quad (2)$$

$$Fe^{3+} + H_2O + h\nu \rightarrow \bullet OH + Fe^{2+} + H^+ \quad (3)$$

As shown in Equation (2), Fe^{2+} rapidly reacts with H_2O_2 to generate Fe^{3+}. The main form of Fe^{3+} is $[Fe(OH)]^{2+}$ at pH 2.8–3.5, which plays a key role in reactions. Subsequently, the reduction of $[Fe(OH)]^{2+}$ under light irradiation achieves redox recycling (Figure 2). Moreover, •OH can be generated via direct photolysis of H_2O_2 [16]. In the photo-Fenton process, the key is to accelerate the reduction of Fe^{3+} to Fe^{2+} via light irradiation. In the heterogeneous photo-Fenton reactions, the active sites' redox cycle determines the reaction rate [114]. Although g-C_3N_4 cannot act as active sites for H_2O_2 decomposition, unique up conversion property, and substantial nitrogen coordinating sites make it become the ideal support for active sites [115]. In addition, the excellent photocatalytic activities of g-C_3N_4 based composites endue unique advantages as a catalyst for photo-Fenton-like reactions [116]. Metal doping into g-C_3N_4 is an important approach to enhance degradation efficiency in photo-Fenton reactions. Fe-doped g-C_3N_4 has been successfully synthesized by thermal shrinkage polymerization for aqueous organic pollutants degradation in photo-Fenton reactions. Introducing Fe in g-C_3N_4 accelerated the separation of photogenerated electron-holes. The Fe accepts electrons towards rapid reduction from trivalent to divalent, promoting the rapid generation of reactive species [117]. Another report about porous Fe-doped g-C_3N_4 revealed that the porous g-C_3N_4 structures enhance the photo-Fenton activity, owing to more active sites (Fe-N4) exposure [118]. An et al. embedded Fe into g-C_3N_4 by pyrolysis of Fe-N-containing precursor and melamine. The high-density Fe-N_x was investigated as a reactive site for H_2O_2 activation [119]. Another strategy used to realize efficient photo-Fenton-based degradation is heterojunction construction, including the Z scheme [120] and type II [121][122]. Zhang et al. prepared MnO_2/Mn-modified alkalinized g-C_3N_4 by the calcination-impregnating method. It was proposed that Z-scheme charge transfer accelerated the redox cycle of the $Mn^{4+}/Mn^{3+}/Mn^{2+}$ [123].

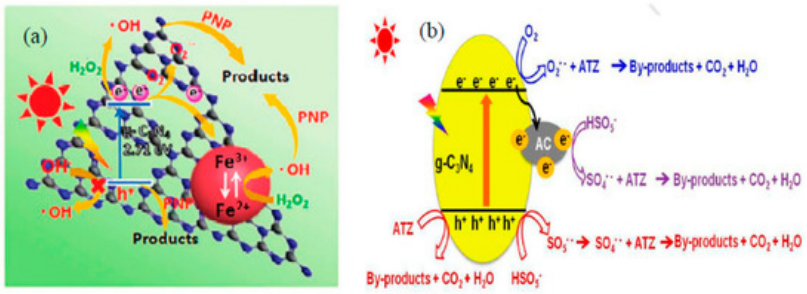

Figure 2. (**a**) schematic illustration of the catalytic mechanism of Fe_2O_3 QDs/g-C_3N_4-900 in H_2O_2/vis system, reprinted with permission from [113]. Copyright 2019 John Wiley & Sons, Inc. (**b**) Mechanism of photocatalytic degradation of atrazine with PMS, reprinted with permission from [96]. Copyright 2018 Elsevier.

3.3. Photo-Assisted Sulfate Radical Based AOPs

Sulfate radical-based advanced oxidation processes (SR-AOPs) are increasingly gaining attention as an effective solution to the destruction of recalcitrant organics in water [124]. Among various approaches to generate sulfate radicals via activation of additional sources of reactive species (such as peroxymonosulfate (PMS) and persulfate (PS)), the photo-activation in the presence of a heterogeneous catalyst is worth mentioning [65]. The general mechanism is presented in Equations (4)–(8).

Photocatalyst + *hv* → e^- + h^+ (4)

$S_2O_8^{2-}$ + e^- → SO_4^{2-} + $SO_4^{\bullet-}$ (5)

HSO_5^- + e^- → $SO_4^{\bullet-}$ + OH^- (6)

HSO_5^- + h^+ → $SO_5^{\bullet-}$ + H^+ (7)

$2SO_5^{\bullet-}$ → $2SO_4^{\bullet-}$ + O_2 (8)

Firstly, photocatalysts are excited under light irradiation to form photo-induced electrons and holes. Then the $\bullet SO_4^-$ and •OH are generated through the combination of electrons and PMS or PS. When transition metals are constructed into photocatalysts, they could be potential reactive sites for PMS/PS activation (shown in Equations (9)–(12)).

M^{n+} + HSO_5^- → $M^{(n+1)+}$ + $SO_4^{\bullet-}$ + OH^- (9)

$M^{(n+1)+}$ + HSO_5^- → M^{n+} + $SO_5^{\bullet-}$ + H^+ (10)

$M^{(n+1)+}$ + e^- → M^{n+} (11)

M^{n+} + h^+ → $M^{(n+1)+}$ (12)

Similar to the application in photo-Fenton-like reactions, g-C_3N_4 generally plays as reactive site supporters or participate in heterojunction construction in photo-assisted sulfate radical based AOPs. The TiO_2/g-C_3N_4 composite was fabricated for paracetamol photocatalytic degradation in the presence of visible light and persulfate. As prepared composite held type II heterojunction, which inhibits the electron-hole recombination in photocatalyst and adding persulfate increased 13 times degradation rate [94]. Liang et al. prepared porous 0D/3D $NiCo_2O_4$/g-C_3N_4 composite for carbamazepine removal. 99% of degradation was achieved in 10 min under visible light irradiation [93]. Jin et al. constructed Z-scheme MoS_2/A g/g-C_3N_4 via a method of chemical electrostatic adsorption. The deposited Ag further enhances photocatalytic activity via improving light utilization ability and the separation rate of photogenerated e^-/h^+ pairs. The results indicated that the presence of PMS dramatically accelerates the photocatalytic reaction [96]. Through metal ions such as Fe and Co doping, enhancing photocatalytic activity and improving PMS activation could synchronize implementation towards an efficient organic pollutant removal [95][98].

References

1. Krasner, S.W. The Formation and Control of Emerging Disinfection by-Products of Health Concern. Philos. Trans. R. Soc. A Math. Phys. Eng. Sci. 2009, 367, 4077–4095.
2. Sauvé, S.; Desrosiers, M. A review of what is an emerging contaminant. Chem. Central J. 2014, 8, 15, doi:10.1186/1752-153x-8-15.
3. Oturan, M.A.; Aaron, J.-J. Advanced Oxidation Processes in Water/Wastewater Treatment: Principles and Applications. A Review. Crit. Rev. Environ. Sci. Technol. 2014, 44, 2577–2641, doi:10.1080/10643389.2013.829765.
4. Luo, Y.; Guo, W.; Ngo, H.H.; Nghiem, L.D.; Hai, F.I.; Zhang, J.; Liang, S.; Wang, X.C. A review on the occurrence of micropollutants in the aquatic environment and their fate and removal during wastewater treatment. Sci. Total. Environ. 2014, 473–474, 619–641, doi:10.1016/j.scitotenv.2013.12.065.
5. Ternes, T.A.; Meisenheimer, M.; McDowell, D.; Sacher, F.; Brauch, H.-J.; Haist-Gulde, B.; Preuss, G.; Wilme, U.; Zulei-Seibert, N. Removal of Pharmaceuticals During Drinking Water Treatment. Environ. Sci. Technol. 2002, 36, 3855–3863.
6. Brown, D.; Laboureur, P. The aerobic biodegradability of primary aromatic amines. Chemosphere 1983, 12, 405–414, doi:10.1016/0045-6535(83)90115-7.

7. Rebhun, M.; Meir, A.S.; Laor, Y. Using Dissolved Humic Acid to Remove Hydrophobic Contaminants from Water by Com-plexation−Flocculation Process. Environ. Sci. Technol. 1998, 32, 981–986, doi:10.1021/es9707163.
8. Laine, D.F.; Cheng, I.F. The destruction of organic pollutants under mild reaction conditions: A review. Microchem. J. 2007, 85, 183–193, doi:10.1016/j.microc.2006.07.002.
9. Anandan, S.; Ponnusamy, V.K.; AshokKumar, M. A review on hybrid techniques for the degradation of organic pollutants in aqueous environment. Ultrason. Sonochemistry 2020, 67, 105130, doi:10.1016/j.ultsonch.2020.105130.
10. Roberto, A.; Caprio, V.; Insola, A.; Marotta, R. Advanced Oxidation Processes (Aop) for Water Purification and Recovery. Catal. Today 1999, 53, 51–59.
11. Herrmann, J.M.; Guillard, C.; Arguello, M.; Agüera, A.; Tejedor, A.; Piedra, L.; Fernández-Alba, A. Photocatalytic Degrada-tion of Pesticide Pirimiphos-Methyl: Determination of the Reaction Pathway and Identification of Intermediate Products by Various Analytical Methods. Catal. Today 1999, 54, 353–367.
12. Gogate, P.R.; Pandit, A.B. A review of imperative technologies for wastewater treatment I: Oxidation technologies at ambient conditions. Adv. Environ. Res. 2004, 8, 501–551, doi:10.1016/s1093-0191(03)00032-7.
13. Gogate, P.R.; Pandit, A.B. A review of imperative technologies for wastewater treatment II: Hybrid methods. Adv. Environ. Res. 2004, 8, 553–597, doi:10.1016/s1093-0191(03)00031-5.
14. Zhang, M.-H.; Dong, H.; Zhao, L.; Wang, D.-X.; Meng, D. A review on Fenton process for organic wastewater treatment based on optimization perspective. Sci. Total. Environ. 2019, 670, 110–121, doi:10.1016/j.scitotenv.2019.03.180.
15. Duesterberg, C.K.; Mylon, S.E.; Waite, T.D. pH Effects on Iron-Catalyzed Oxidation using Fenton's Reagent. Environ. Sci. Technol. 2008, 42, 8522–8527, doi:10.1021/es801720d.
16. Pignatello, J.J.; Oliveros, E.; Mackay, A. Advanced Oxidation Processes for Organic Contaminant Destruction Based on the Fenton Reaction and Related Chemistry. Crit. Rev. Environ. Sci. Technol. 2006, 36, 1–84, doi:10.1080/10643380500326564.
17. Klavarioti, M.; Mantzavinos, D.; Fatta-Kassinos, D. Removal of residual pharmaceuticals from aqueous systems by advanced oxidation processes. Environ. Int. 2009, 35, 402–417, doi:10.1016/j.envint.2008.07.009.
18. Esplugas, S.; Giménez, J.; Contreras, S.; Pascual, E.; RodríguezM. Comparison of different advanced oxidation processes for phenol degradation. Water Res. 2002, 36, 1034–1042, doi:10.1016/s0043-1354(01)00301-3.
19. Bokare, A.D.; Choi, W. Singlet-Oxygen Generation in Alkaline Periodate Solution. Environ. Sci. Technol. 2015, 49, 14392–14400, doi:10.1021/acs.est.5b04119.
20. Ye, T.; Wei, Z.; Spinney, R.; Dionysiou, D.D.; Luo, S.; Chai, L.; Yang, Z.-H.; Xiao, R. Quantitative structure–activity relation-ship for the apparent rate constants of aromatic contaminants oxidized by ferrate (VI). Chem. Eng. J. 2017, 317, 258–266, doi:10.1016/j.cej.2017.02.061.
21. Trojanowicz, M. Removal of persistent organic pollutants (POPs) from waters and wastewaters by the use of ionizing radia-tion. Sci. Total. Environ. 2020, 718, 134425, doi:10.1016/j.scitotenv.2019.134425.
22. Shah, N.S.; Khan, J.A.; Sayed, M.; Khan, Z.U.H.; Iqbal, J.; Arshad, S.; Junaid, M.; Khan, H.M. Synergistic effects of H2O2 and S2O82− in the gamma radiation induced degradation of congo-red dye: Kinetics and toxicities evaluation. Sep. Purif. Technol. 2020, 233, 115966, doi:10.1016/j.seppur.2019.115966.
23. Buthiyappan, A.; Aziz, A.R.A.; Wan, M.A.W.D. Recent Advances and Prospects of Catalytic Advanced Oxidation Process in Treating Textile Effluents. Rev. Chem. Eng. 2016, 32, 1–47.
24. Zhu, J.; Xiao, P.; Li, H.; Carabineiro, S.A.C. Graphitic Carbon Nitride: Synthesis, Properties, and Applications in Catalysis. ACS Appl. Mater. Interfaces 2014, 6, 16449–16465, doi:10.1021/am502925j.
25. Ong, W.-J.; Tan, L.-L.; Lling-Lling, T.; Yong, S.-T.; Chai, S.-P. Graphitic Carbon Nitride (g-C3N4)-Based Photocatalysts for Artificial Photosynthesis and Environmental Remediation: Are We a Step Closer To Achieving Sustainability? Chem. Rev. 2016, 116, 7159–7329, doi:10.1021/acs.chemrev.6b00075.
26. Wang, X.; Maeda, K.; Thomas, A.; Takanabe, K.; Xin, G.; Carlsson, J.M.; Domen, K.; Antonietti, M. A metal-free polymeric photocatalyst for hydrogen production from water under visible light. Nat. Mater. 2009, 8, 76–80.
27. Xu, J.; Zhang, L.; Shi, R.; Zhu, Y. Chemical exfoliation of graphitic carbon nitride for efficient heterogeneous photocatalysis. J. Mater. Chem. A 2013, 1, 14766–14772, doi:10.1039/c3ta13188b.
28. Cui, Y.; Ding, Z.; Liu, P.; Antonietti, M.; Fu, X.; Wang, X. Metal-Free Activation of H2O2 by g-C3N4 under Visible Light Irra-diation for the Degradation of Organic Pollutants. Phys. Chem. Chem. Phys. 2012, 14, 1455–1462.
29. Liebig, J. Uber einige Stickstoff—Verbindungen. Ann. Pharm. 1834, 10, 1–47, doi:10.1002/jlac.18340100102.

30. Goettmann, F.; Fischer, A.; Antonietti, M.; Thomas, A. Metal-free catalysis of sustainable Friedel–Crafts reactions: Direct activation of benzene by carbon nitrides to avoid the use of metal chlorides and halogenated compounds. Chem. Commun. 2006, 4530–4532, doi:10.1039/b608532f.

31. Sudhaik, A.; Raizada, P.; Shandilya, P.; Jeong, D.-Y.; Lim, J.-H.; Singh, P. Review on fabrication of graphitic carbon nitride based efficient nanocomposites for photodegradation of aqueous phase organic pollutants. J. Ind. Eng. Chem. 2018, 67, 28–51, doi:10.1016/j.jiec.2018.07.007.

32. Kumar, S.; Karthikeyan, S.; Lee, A.F. g-C3N4-Based Nanomaterials for Visible Light-Driven Photocatalysis. Catalysts 2018, 8, 74, doi:10.3390/catal8020074.

33. Zhang, S.; Li, J.; Wang, X.; Huang, Y.; Zeng, M.; Xu, J. Rationally Designed 1d Ag@AgVO3 Nanowire/Graphene/Protonated g-C3N4 Nanosheet Heterojunctions for Enhanced Photocatalysis Via Electrostatic Self-Assembly and Photochemical Reduc-tion Methods. J. Mater. Chem. A 2015, 3, 10119–10126.

34. Ye, C.; Li, J.-X.; Li, Z.-J.; Li, X.-B.; Fan, X.-B.; Zhang, L.-P.; Chen, B.; Tung, C.; Wu, L. Enhanced Driving Force and Charge Separation Efficiency of Protonated g-C3N4 for Photocatalytic O2 Evolution. ACS Catal. 2015, 5, 6973–6979, doi:10.1021/acscatal.5b02185.

35. Bai, X.; Wang, L.; Zong, R.; Zhu, Y. Photocatalytic Activity Enhanced via g-C3N4 Nanoplates to Nanorods. J. Phys. Chem. C 2013, 117, 9952–9961, doi:10.1021/jp402062d.

36. Xu, J.; Wang, Y.; Zhu, Y. Nanoporous Graphitic Carbon Nitride with Enhanced Photocatalytic Performance. Langmuir 2013, 29, 10566–10572, doi:10.1021/la402268u.

37. Zhang, M.; Xu, J.; Zong, R.; Liu, D. Enhancement of visible light photocatalytic activities via porous structure of g-C3N4. Appl. Catal. B Environ. 2014, 147, 229–235, doi:10.1016/j.apcatb.2013.09.002.

38. Chen, X.; Zhang, J.; Fu, X.; Antonietti, M.; Wang, X. Fe-g-C3N4-Catalyzed Oxidation of Benzene to Phenol Using Hydrogen Peroxide and Visible Light. J. Am. Chem. Soc. 2009, 131, 11658–11659, doi:10.1021/ja903923s.

39. Zhang, M.; Bai, X.; Liu, D.; Wang, J.; Liu, D. Enhanced catalytic activity of potassium-doped graphitic carbon nitride induced by lower valence position. Appl. Catal. B Environ. 2015, 164, 77–81, doi:10.1016/j.apcatb.2014.09.020.

40. Yan, S.; Yan, S.; Wang, J.; Huang, Y.A.; Wang, P.; Li, Z.; Zou, Z. Towards efficient solar hydrogen production by intercalated carbon nitride photocatalyst. Phys. Chem. Chem. Phys. 2013, 15, 18077–18084, doi:10.1039/c3cp53774a.

41. Wang, X.; Chen, X.; Thomas, A.; Fu, X.; Antonietti, M. Metal-Containing Carbon Nitride Compounds: A New Functional Organic-Metal Hybrid Material. Adv. Mater. 2009, 21, 1609–1612, doi:10.1002/adma.200802627.

42. Yan, S.; Yan, S.; Wang, J.; Zou, Z. Ion coordination significantly enhances the photocatalytic activity of graphitic-phase car-bon nitride. Dalton Trans. 2014, 43, 8178–8183, doi:10.1039/c3dt53224k.

43. Hu, S.; Ma, L.; You, J.; Li, F.; Fan, Z.; Lu, G.; Liu, D.; Gui, J. Enhanced visible light photocatalytic performance of g-C3N4 photocatalysts co-doped with iron and phosphorus. Appl. Surf. Sci. 2014, 311, 164–171, doi:10.1016/j.apsusc.2014.05.036.

44. Pan, H.; Zhang, Y.-W.; Shenoy, V.B.; Gao, H. Ab Initio Study on a Novel Photocatalyst: Functionalized Graphitic Carbon Nitride Nanotube. ACS Catal. 2011, 1, 99–104, doi:10.1021/cs100045u.

45. Liu, G.; Niu, P.; Sun, C.; Smith, S.C.; Chen, Z.; Lu, G.Q.; Cheng, H.-M. Unique Electronic Structure Induced High Photoreac-tivity of Sulfur-Doped Graphitic C3N4. J. Am. Chem. Soc. 2010, 132, 11642–11648, doi:10.1021/ja103798k.

46. Zhang, S.; Li, J.; Zeng, M.; Li, J.; Xu, J.; Wang, X. Bandgap Engineering and Mechanism Study of Nonmetal and Metal Ion Codoped Carbon Nitride: C+Fe as an Example. Chem.-A Eur. J. 2014, 20, 9805–9812, doi:10.1002/chem.201400060.

47. Ma, X.; Lv, Y.; Xu, J.; Liu, Y.; Zhang, R.; Zhu, Y. A Strategy of Enhancing the Photoactivity of g-C3N4 via Doping of Nonmet-al Elements: A First-Principles Study. J. Phys. Chem. C 2012, 116, 23485–23493, doi:10.1021/jp308334x.

48. Zhang, G.; Zhang, M.; Ye, X.; Qiu, X.; Lin, S.; Wang, X. Iodine Modified Carbon Nitride Semiconductors as Visible Light Photocatalysts for Hydrogen Evolution. Adv. Mater. 2014, 26, 805–809, doi:10.1002/adma.201303611.

49. Wang, Y.; Di, Y.; Antonietti, M.; Li, H.; Chen, X.; Wang, X. Excellent Visible-Light Photocatalysis of Fluorinated Polymeric Carbon Nitride Solids. Chem. Mater. 2010, 22, 5119–5121, doi:10.1021/cm1019102.

50. Yan, S.C.; Li, Z.S.; Zou, Z.G. Photodegradation of Rhodamine B and Methyl Orange over Boron-Doped g-C3N4under Visible Light Irradiation. Langmuir 2010, 26, 3894–3901, doi:10.1021/la904023j.

51. Di, J.; Xia, J.; Xia, J.; Xu, H.; Xu, L.; Xu, Y.; He, M.; Li, H. Preparation of sphere-like g-C3N4/BiOI photocatalysts via a reac-table ionic liquid for visible-light-driven photocatalytic degradation of pollutants. J. Mater. Chem. A 2014, 2, 5340–5351, doi:10.1039/c3ta14617k.

52. Sui, Y.; Liu, J.; Zhang, Y.; Tian, X.; Chen, W. Dispersed conductive polymer nanoparticles on graphitic carbon nitride for enhanced solar-driven hydrogen evolution from pure water. Nanoscale 2013, 5, 9150–9155, doi:10.1039/c3nr02413j.

53. He, F.; Chen, G.; Yu, Y.; Hao, S.; Zhou, Y.; Zheng, Y. Facile Approach to Synthesize g-PAN/g-C3N4 Composites with En-hanced Photocatalytic H2 Evolution Activity. ACS Appl. Mater. Interfaces 2014, 6, 7171–7179, doi:10.1021/am500198y.

54. Jin, Z.; Murakami, N.; Tsubota, T.; Ohno, T. Complete oxidation of acetaldehyde over a composite photocatalyst of graphitic carbon nitride and tungsten(VI) oxide under visible-light irradiation. Appl. Catal. B Environ. 2014, 150–151, 479–485, doi:10.1016/j.apcatb.2013.12.048.

55. Sridharan, K.; Jang, E.; Park, T.J. Novel visible light active graphitic C3N4–TiO2 composite photocatalyst: Synergistic synthesis, growth and photocatalytic treatment of hazardous pollutants. Appl. Catal. B: Environ. 2013, 142–143, 718–728, doi:10.1016/j.apcatb.2013.05.077.

56. Miranda, C.; Mansilla, H.; Yáñez, J.; Obregón, S.; Colon, G. Improved photocatalytic activity of g-C3N4/TiO2 composites prepared by a simple impregnation method. J. Photochem. Photobiol. A Chem. 2013, 253, 16–21, doi:10.1016/j.jphotochem.2012.12.014.

57. Zhou, X.; Jin, B.; Li, L.; Peng, F.; Wang, H.; Yu, H.; Fang, Y. A carbon nitride/TiO2 nanotube array heterojunction visible-light photocatalyst: Synthesis, characterization, and photoelectrochemical properties. J. Mater. Chem. 2012, 22, 17900–17905, doi:10.1039/c2jm32686h.

58. Fan, X.; Zhang, L.; Wang, M.; Huang, W.; Zhou, Y.; Li, M.; Cheng, R.; Shi, J. Constructing carbon-nitride-based copolymers via Schiff base chemistry for visible-light photocatalytic hydrogen evolution. Appl. Catal. B Environ. 2016, 182, 68–73, doi:10.1016/j.apcatb.2015.09.006.

59. Chen, Z.; Pronkin, S.; Fellinger, T.-P.; Kailasam, K.; Vilé, G.; Albani, D.; Krumeich, F.; Leary, R.; Barnard, J.; Thomas, J.M.; et al. Merging Single-Atom-Dispersed Silver and Carbon Nitride to a Joint Electronic System via Copolymerization with Silver Tricyanomethanide. ACS Nano 2016, 10, 3166–3175, doi:10.1021/acsnano.5b04210.

60. Zhang, J.; Chen, X.; Takanabe, K.; Maeda, K.; Domen, K.; Epping, J.D.; Fu, X.; Antonietti, M.; Wang, X. Synthesis of a Carbon Nitride Structure for Visible-Light Catalysis by Copolymerization. Angew. Chem. Int. Ed. 2010, 49, 441–444.

61. Zhang, M.; Yao, W.; Lv, Y.; Bai, X.; Liu, Y.; Jiang, W.; Zhu, Y. Enhancement of mineralization ability of C3N4via a lower va-lence position by a tetracyanoquinodimethane organic semiconductor. J. Mater. Chem. A 2014, 2, 11432–11438, doi:10.1039/c4ta01471e.

62. Jin, J.; Sun, K.; Wu, F.; Gao, B.; Wang, Z.; Kang, M.; Bai, Y.; Zhao, Y.; Liu, X.; Xing, B. Single-solute and bi-solute sorption of phenanthrene and dibutyl phthalate by plant- and manure-derived biochars. Sci. Total. Environ. 2014, 473–474, 308–316, doi:10.1016/j.scitotenv.2013.12.033.

63. Han, L.; Ro, K.S.; Sun, K.; Sun, H.; Wang, Z.; Libra, J.A.; Xing, B. New Evidence for High Sorption Capacity of Hydrochar for Hydrophobic Organic Pollutants. Environ. Sci. Technol. 2016, 50, 13274–13282, doi:10.1021/acs.est.6b02401.

64. Iervolino, G.; Zammit, I.; Vaiano, V.; Rizzo, L. Limitations and Prospects for Wastewater Treatment by UV and Visi-ble-Light-Active Heterogeneous Photocatalysis: A Critical Review. Top. Curr. Chem. 2019, 378, 7, doi:10.1007/s41061-019-0272-1.

65. Yang, Q.; Ma, Y.; Chen, F.; Yao, F.; Sun, J.; Wang, S.; Yi, K.; Hou, L.; Li, X.; Wang, D. Recent advances in photo-activated sulfate radical-advanced oxidation process (SR-AOP) for refractory organic pollutants removal in water. Chem. Eng. J. 2019, 378, 122149, doi:10.1016/j.cej.2019.122149.

66. Gao, Y.; Zhu, Y.; Lyu, L.; Zeng, Q.; Xing, X.; Hu, C. Electronic Structure Modulation of Graphitic Carbon Nitride by Oxygen Doping for Enhanced Catalytic Degradation of Organic Pollutants through Peroxymonosulfate Activation. Environ. Sci. Technol. 2018, 52, 14371–14380, doi:10.1021/acs.est.8b05246.

67. Li, H.; Shan, C.; Panab, B. Fe(III)-Doped g-C3N4 Mediated Peroxymonosulfate Activation for Selective Degradation of Phe-nolic Compounds via High-Valent Iron-Oxo Species. Environ. Sci. Technol. 2018, 52, 2197–2205, doi:10.1021/acs.est.7b05563.

68. Ding, Q.; Lam, F.L.; Hu, X. Complete degradation of ciprofloxacin over g-C3N4-iron oxide composite via heterogeneous dark Fenton reaction. J. Environ. Manag. 2019, 244, 23–32, doi:10.1016/j.jenvman.2019.05.035.

69. Fang, L.; Liu, Z.; Zhou, C.; Guo, Y.; Feng, Y.; Yang, M. Degradation Mechanism of Methylene Blue by H2O2 and Synthesized Carbon Nanodots/Graphitic Carbon Nitride/Fe(II) Composite. J. Phys. Chem. C 2019, 123, 26921–26931, doi:10.1021/acs.jpcc.9b06774.

70. Chen, Z.; Zhang, S.; Liu, Y.; Alharbi, N.S.; Rabah, S.O.; Wang, S.; Wang, X. Synthesis and fabrication of g-C3N4-based mate-rials and their application in elimination of pollutants. Sci. Total. Environ. 2020, 731, 139054,

doi:10.1016/j.scitotenv.2020.139054.

71. Jiang, W.; Luo, W.; Wang, J.; Zhang, M.; Liu, D. Enhancement of catalytic activity and oxidative ability for graphitic carbon nitride. J. Photochem. Photobiol. C: Photochem. Rev. 2016, 28, 87–115, doi:10.1016/j.jphotochemrev.2016.06.001.
72. Oh, W.-D.; Dong, Z.; Lim, T.-T. Generation of sulfate radical through heterogeneous catalysis for organic contaminants re-moval: Current development, challenges and prospects. Appl. Catal. B: Environ. 2016, 194, 169–201, doi:10.1016/j.apcatb.2016.04.003.
73. Hu, P.; Long, M. Cobalt-catalyzed sulfate radical-based advanced oxidation: A review on heterogeneous catalysts and ap-plications. Appl. Catal. B: Environ. 2016, 181, 103–117, doi:10.1016/j.apcatb.2015.07.024.
74. Kasprzyk-Hordern, B.; Ziółek, M.; Nawrocki, J. Catalytic ozonation and methods of enhancing molecular ozone reactions in water treatment. Appl. Catal. B: Environ. 2003, 46, 639–669, doi:10.1016/s0926-3373(03)00326-6.
75. Lyu, L.; Yan, D.; Yu, G.; Cao, W.; Hu, C. Efficient Destruction of Pollutants in Water by a Dual-Reaction-Center Fenton-Like Process over Carbon Nitride Compounds-Complexed Cu(II)-CuAlO2. Environ. Sci. Technol. 2018, 52, 4294–4304.
76. Zhou, C.; Liu, Z.; Fang, L.; Guo, Y.; Feng, Y.; Yang, M. Kinetic and Mechanistic Study of Rhodamine B Degradation by H2O2 and Cu/Al2O3/ g-C3N4 Composite. Catalysts 2020, 10, 317.
77. Guo, F.; Lu, J.; Liu, Q.; Zhang, P.; Zhang, A.; Cai, Y.; Wang, Q. Degradation of Acid Orange 7 by peroxymonosulfate acti-vated with the recyclable nanocomposites of g-C3N4 modified magnetic carbon. Chemosphere 2018, 205, 297–307, doi:10.1016/j.chemosphere.2018.04.139.
78. Pi, Y.; Gao, H.; Cao, Y.; Cao, R.; Wang, Y.; Sun, J. Cobalt ferrite supported on carbon nitride matrix prepared using waste battery materials as a peroxymonosulfate activator for the degradation of levofloxacin hydrochloride. Chem. Eng. J. 2020, 379, 122377, doi:10.1016/j.cej.2019.122377.
79. Xie, M.; Tang, J.; Kong, L.; Lu, W.; Natarajan, V.; Zhu, F.; Zhan, J. Cobalt doped g-C3N4 activation of peroxymonosulfate for monochlorophenols degradation. Chem. Eng. J. 2019, 360, 1213–1222, doi:10.1016/j.cej.2018.10.130.
80. Fan, J.; Qin, H.; Jiang, S. Mn-doped g-C3N4 composite to activate peroxymonosulfate for acetaminophen degradation: The role of superoxide anion and singlet oxygen. Chem. Eng. J. 2019, 359, 723–732, doi:10.1016/j.cej.2018.11.165.
81. Ma, J.; Jia, N.; Shen, C.; Liu, W.; Wen, Y. Stable cuprous active sites in Cu+-graphitic carbon nitride: Structure analysis and performance in Fenton-like reactions. J. Hazard. Mater. 2019, 378, 120782, doi:10.1016/j.jhazmat.2019.120782.
82. Wang, Y.; Cao, D.; Liu, M.; Zhao, X. Insights into heterogeneous catalytic activation of peroxymonosulfate by Pd/g-C3N4: The role of superoxide radical and singlet oxygen. Catal. Commun. 2017, 102, 85–88, doi:10.1016/j.catcom.2017.08.016.
83. Wang, S.; Liu, Y.; Wang, J. Iron and Sulfur Co-Doped Graphite Carbon Nitride (FeOy/S-g-C3N4) for Activating Peroxymo-nosulfate to Enhance Sulfamethoxazole Degradation. Chem. Eng. J. 2020, 382, 122836.
84. Oh, W.-D.; Ng, C.-Z.; Ng, S.L.; Lim, J.-W.; Leong, K.-H. Rapid degradation of organics by peroxymonosulfate activated with ferric ions embedded in graphitic carbon nitride. Sep. Purif. Technol. 2020, 230, 115852, doi:10.1016/j.seppur.2019.115852.
85. Li, J.; Fang, J.; Gao, L.; Zhang, J.; Ruan, X.; Xu, A.; Li, X. Graphitic carbon nitride induced activity enhancement of OMS-2 catalyst for pollutants degradation with peroxymonosulfate. Appl. Surf. Sci. 2017, 402, 352–359, doi:10.1016/j.apsusc.2017.01.129.
86. Zhu, Y.; Chen, Z.; Gao, Y.; Hu, C. General synthesis of carbon and oxygen dual-doped graphitic carbon nitride via copoly-merization for non-photochemical oxidation of organic pollutant. J. Hazard. Mater. 2020, 394, 122578, doi:10.1016/j.jhazmat.2020.122578.
87. Wei, M.; Gao, L.; Li, J.; Fang, J.; Cai, W.; Li, X.; Xu, A. Activation of peroxymonosulfate by graphitic carbon nitride loaded on activated carbon for organic pollutants degradation. J. Hazard. Mater. 2016, 316, 60–68, doi:10.1016/j.jhazmat.2016.05.031.
88. Li, H.; Shan, C.; Panab, B. Development of Fe-doped g-C3N4/graphite mediated peroxymonosulfate activation for degrada-tion of aromatic pollutants via nonradical pathway. Sci. Total. Environ. 2019, 675, 62–72, doi:10.1016/j.scitotenv.2019.04.171.
89. Feng, Y.; Liao, C.-Z.; Kong, L.; Wu, D.; Liu, Y.; Lee, P.-H.; Shih, K. Facile synthesis of highly reactive and stable Fe-doped g-C3N4 composites for peroxymonosulfate activation: A novel nonradical oxidation process. J. Hazard. Mater. 2018, 354, 63–71, doi:10.1016/j.jhazmat.2018.04.056.

90. Chen, C.; Xie, M.; Kong, L.; Lu, W.; Feng, Z.; Zhan, J. Mn3O4 Nanodots Loaded g-C3N4 Nanosheets for Catalytic Membrane Degradation of Organic Contaminants. J. Hazard. Mater. 2020, 390,122146.

91. Oh, W.-D.; Chang, V.W.; Hu, Z.-T.; Goei, R.; Lim, T.-T. Enhancing the catalytic activity of g-C3N4 through Me doping (Me = Cu, Co and Fe) for selective sulfathiazole degradation via redox-based advanced oxidation process. Chem. Eng. J. 2017, 323, 260–269, doi:10.1016/j.cej.2017.04.107.

92. Qin, Z.; Wang, M.; Li, R.; Chen, Y. Novel Cu3P/g-C3N4 p-n heterojunction photocatalysts for solar hydrogen generation. Sci. China Mater. 2018, 61, 861–868, doi:10.1007/s40843-017-9171-9.

93. Jiang, J.; Wang, X.; Zhang, C.; Li, T.; Lin, Y.; Xie, T.; Dong, S. Porous 0d/3d NiCo2O4/g-C3N4 Accelerate Emerging Pollutant Degradation in PMS/Vis System: Degradation Mechanism, Pathway and Toxicity Assessment. Chem. Eng. J. 2020, 397, 125356.

94. Du, X.; Bai, X.; Xu, L.; Yang, L.; Jin, P. Visible-Light Activation of Persulfate by TiO2/ g-C3N4 Photocatalyst toward Efficient Degradation of Micropollutants. Chem. Eng. J. 2020, 384, 123245.

95. Li, R.; Huang, J.; Cai, M.; Huang, J.; Xie, Z.; Zhang, Q.; Liu, Y.; Liu, H.; Lv, W.; Liu, G. Activation of peroxymonosulfate by Fe doped g-C3N4 /graphene under visible light irradiation for Trimethoprim degradation. J. Hazard. Mater. 2020, 384, 121435, doi:10.1016/j.jhazmat.2019.121435.

96. Jin, C.; Kang, J.; Li, Z.; Wang, M.; Wu, Z.; Xie, Y. Enhanced visible light photocatalytic degradation of tetracycline by MoS2/Ag/g-C3N4 Z-scheme composites with peroxymonosulfate. Appl. Surf. Sci. 2020, 514, 146076, doi:10.1016/j.apsusc.2020.146076.

97. Dikdim, J.M.D.; Gong, Y.; Noumi, G.B.; Sieliechi, J.M.; Zhao, X.; Ma, N.; Yang, M.; Tchatchueng, J.B. Peroxymonosulfate improved photocatalytic degradation of atrazine by activated carbon/graphitic carbon nitride composite under visible light irradiation. Chemosphere 2019, 217, 833–842, doi:10.1016/j.chemosphere.2018.10.177.

98. Wang, L.; Guo, X.; Chen, Y.; Ai, S.; Ding, H. Cobalt-doped g-C3N4 as a heterogeneous catalyst for photo-assisted activation of peroxymonosulfate for the degradation of organic contaminants. Appl. Surf. Sci. 2019, 467–468, 954–962, doi:10.1016/j.apsusc.2018.10.262.

99. Lin, K.-Y.A.; Zhang, Z.-Y. Degradation of Bisphenol A using peroxymonosulfate activated by one-step prepared sulfur-doped carbon nitride as a metal-free heterogeneous catalyst. Chem. Eng. J. 2017, 313, 1320–1327, doi:10.1016/j.cej.2016.11.025.

100. Dong, L.; Xu, T.; Chen, W.; Lu, W. Synergistic multiple active species for the photocatalytic degradation of contaminants by imidazole-modified g-C3N4 coordination with iron phthalocyanine in the presence of peroxymonosulfate. Chem. Eng. J. 2019, 357, 198–208, doi:10.1016/j.cej.2018.09.094.

101. Dong, Q.; Chen, Y.; Wang, L.; Ai, S.; Ding, H. Cu-modified alkalinized g -C 3 N 4 as photocatalytically assisted heterogene-ous Fenton-like catalyst. Appl. Surf. Sci. 2017, 426, 1133–1140, doi:10.1016/j.apsusc.2017.07.254.

102. Fujishima, A.; Honda, K. Electrochemical Photolysis of Water at a Semiconductor Electrode. Natature 1972, 238, 37–38, doi:10.1038/238037a0.

103. Kumar, A.; Kumar, A.; Sharma, G.; Ala'a, H.; Naushad, M.; Ghfar, A.A.; Stadler, F.J. Quaternary Magnetic Biocl/ g-C3N4/Cu2O/Fe3O4 Nano-Junction for Visible Light and Solar Powered Degradation of Sulfamethoxazole from Aqueous En-vironment. Chem. Eng. J. 2018, 334, 462–478.

104. Kumar, A.; Sharma, S.K.; Sharma, G.; Naushad, M.; Stadler, F.J. CeO2/ g-C3N4/V2O5 Ternary Nano Hetero-Structures Deco-rated with Cqds for Enhanced Photo-Reduction Capabilities under Different Light Sources: Dual Z-Scheme Mechanism. J. Alloy. Compd. 2020, 838, 155692.

105. Tay, Q.; Kanhere, P.D.; Ng, C.F.; Chen, S.; Chakraborty, S.; Huan, A.C.H.; Sum, T.C.; Ahuja, R.; Chen, Z. Defect Engineered g-C3N4 for Efficient Visible Light Photocatalytic Hydrogen Production. Chem. Mater. 2015, 27, 4930–4933, doi:10.1021/acs.chemmater.5b02344.

106. Duan, J.; Chen, S.; Jaroniec, M.; Qiao, S.Z. Porous C3N4Nanolayers@N-Graphene Films as Catalyst Electrodes for Highly Efficient Hydrogen Evolution. ACS Nano 2015, 9, 931–940, doi:10.1021/nn506701x.

107. Zhao, Y.; Zhao, F.; Wang, X.; Xu, C.; Zhang, Z.; Shi, G.; Qu, L. Graphitic Carbon Nitride Nanoribbons: Graphene-Assisted Formation and Synergic Function for Highly Efficient Hydrogen Evolution. Angew. Chem. Int. Ed. 2014, 53, 13934–13939, doi:10.1002/anie.201409080.

108. Yu, J.C.; Yu, J.C.; Shen, Z.; Chan, D.K.L.; Gu, T. g-C3N4 quantum dots: Direct synthesis, upconversion properties and photo-catalytic application. Chem. Commun. 2014, 50, 10148–10150, doi:10.1039/c4cc02543a.

109. Iqbal, J.; Shah, N.S.; Sayed, M.; Imran, M.; Muhammad, N.; Howari, F.M.; Alkhoori, S.A.; Khan, J.A.; Khan, Z.U.H.; Bhatnagar, A.; et al. Synergistic effects of activated carbon and nano-zerovalent copper on the performance of

hydroxyap-atite-alginate beads for the removal of As3+ from aqueous solution. J. Clean. Prod. 2019, 235, 875–886, doi:10.1016/j.jclepro.2019.06.316.

110. Kumarab, A.; Kumarib, A.; Sharmaab, G.; Dua, B.; Naushad, M.; Stadler, F.J. Carbon quantum dots and reduced graphene oxide modified self-assembled S@C3N4/B@C3N4 metal-free nano-photocatalyst for high performance degradation of chloram-phenicol. J. Mol. Liq. 2020, 300, 112356, doi:10.1016/j.molliq.2019.112356.
111. Liu, Y.; Wang, R.; Yang, Z.; Du, H.; Jiang, Y.; Shen, C.; Liang, K.; Xu, A.-W. Enhanced visible-light photocatalytic activity of Z-scheme graphitic carbon nitride/oxygen vacancy-rich zinc oxide hybrid photocatalysts. Chin. J. Catal. 2015, 36, 2135–2144, doi:10.1016/s1872-2067(15)60985-8.
112. Yu, W.; Xu, D.; Peng, T. Enhanced photocatalytic activity of g-C3N4 for selective CO2 reduction to CH3OH via facile cou-pling of ZnO: A direct Z-scheme mechanism. J. Mater. Chem. A 2015, 3, 19936–19947, doi:10.1039/c5ta05503b.
113. Hernandez, R.; Zappi, M.E.; Colucci, J.; Jones, R. Comparing the performance of various advanced oxidation processes for treatment of acetone contaminated water. J. Hazard. Mater. 2002, 92, 33–50, doi:10.1016/s0304-3894(01)00371-5.
114. Xi, J.; Xia, H.; Ning, X.; Zhang, Z.; Liu, J.; Mu, Z.; Zhang, S.; Du, P.; Lu, X. Carbon-Intercalated 0D/2D Hybrid of Hematite Quantum Dots/Graphitic Carbon Nitride Nanosheets as Superior Catalyst for Advanced Oxidation. Small 2019, 15, e1902744, doi:10.1002/smll.201902744.
115. Wen, J.; Xie, J.; Chen, X.; Li, X. A review on g-C3N4-based photocatalysts. Appl. Surf. Sci. 2017, 391, 72–123, doi:10.1016/j.apsusc.2016.07.030.
116. Mamba, G.; Mishra, A. Graphitic carbon nitride (g-C3N4) nanocomposites: A new and exciting generation of visible light driven photocatalysts for environmental pollution remediation. Appl. Catal. B Environ. 2016, 198, 347–377, doi:10.1016/j.apcatb.2016.05.052.
117. Hu, J.; Zhang, P.; An, W.; Liu, L.; Liang, Y.; Cui, W. In-situ Fe-doped g-C3N4 heterogeneous catalyst via photocataly-sis-Fenton reaction with enriched photocatalytic performance for removal of complex wastewater. Appl. Catal. B Environ. 2019, 245, 130–142, doi:10.1016/j.apcatb.2018.12.029.
118. Miao, W.; Liu, Y.; Chen, X.; Zhao, Y.; Mao, S. Tuning layered Fe-doped g-C3N4 structure through pyrolysis for enhanced Fenton and photo-Fenton activities. Carbon 2020, 159, 461–470, doi:10.1016/j.carbon.2019.12.056.
119. An, S.; Zhang, G.; Wang, T.; Zhang, W.; Li, K.; Song, C.; Miller, J.T.; Miao, S.; Wang, J.; Guo, X. High-Density Ultra-small Clusters and Single-Atom Fe Sites Embedded in Graphitic Carbon Nitride (g-C3N4) for Highly Efficient Catalytic Advanced Oxidation Processes. ACS Nano 2018, 12, 9441–9450, doi:10.1021/acsnano.8b04693.
120. Raizada, P.; Khan, A.A.P.; Singh, P. Construction of carbon nanotube mediated Fe doped graphitic carbon nitride and Ag3VO4 based Z-scheme heterojunction for H2O2 assisted 2,4 dimethyl phenol photodegradation. Sep. Purif. Technol. 2020, 247, 116957, doi:10.1016/j.seppur.2020.116957.
121. Wang, H.; Xu, Y.; Jing, L.; Huang, S.; Li, H.; He, M.; Xu, H.; Li, H. Novel magnetic BaFe12O19/g-C3N4 composites with en-hanced thermocatalytic and photo-Fenton activity under visible-light. J. Alloy. Compd. 2017, 710, 510–518, doi:10.1016/j.jallcom.2017.03.144.
122. Yoon, M.; Oh, Y.; Hong, S.; Lee, J.S.; Boppella, R.; Kim, S.H.; Mota, F.M.; Kim, S.O.; Kim, D.H. Synergistically enhanced photocatalytic activity of graphitic carbon nitride and WO3 nanohybrids mediated by photo-Fenton reaction and H2O2. Appl. Catal. B Environ. 2017, 206, 263–270, doi:10.1016/j.apcatb.2017.01.038.
123. Zhang, Q.; Peng, Y.; Deng, F.; Wang, M.; Chen, D. Porous Z-scheme MnO2/Mn-modified Alkalinized g-C3N4 Heterojunction with Excellent Fenton-like Photocatalytic Activity for Efficient Degradation of Pharmaceutical Pollutants. Sep. Purif. Technol. 2020, 246, 116890, doi:10.1016/j.seppur.2020.116890
124. Anipsitakis, G.P.; Dionysiou, D.D. Degradation of Organic Contaminants in Water with Sulfate Radicals Generated by the Conjunction of Peroxymonosulfate with Cobalt. Environ. Sci. Technol. 2003, 37, 4790–4797, doi:10.1021/es0263792.